Analytical method for band structure calculation of photonic crystal fibers filled with liquid crystal

Juan Juan Hu[1,*], Guobin Ren[1], Ping Shum[1], Xia Yu[1], Guanghui Wang[1], and Chao Lu[2]

[1]*School of Electrical and Electronic Engineering, Nanyang Technological University, Singapore*
[2]*Department of Electronic and Information Engineering, Hong Kong Polytechnic University, Hong Kong*
**Corresponding author: hujuanjuan@pmail.ntu.edu.sg*

Abstract: An analytical method for band structure calculations of photonic crystal fibers with liquid crystal infiltrations is presented. The scalar eigenvalue equation is extended to treat both isotropic and anisotropic materials by introducing a coefficient to describe the index contrast between the extraordinary and ordinary refractive index of the liquid crystal. The simple model provides a fast insight into bandgap formation in photonic crystal fibers filled with anisotropic material such as liquid crystal, which would be useful to aid the design based on such fibers.

OCIS codes: (060.2280) Fiber design and fabrication; (060.2400) Fiber properties.

References and links

1. J. C.Knight, T. A. Birks, P. St. J. Russell, and D. M. Atkin, "All-silica single-mode optical fiber with photonic crystal cladding," Opt. Lett. **21**, 1547-1549 (1996).
2. P. St. J. Russell, "Photonic crystal fibers," J. Lightwave Technol. **24**, 4729-4749 (2006).
3. R. T. Bise, R. S. Windeler, K. S. Kranz, C. Kerbage, B. J. Eggleton, and D. J. Trevor, "Tunable photonic band gap fiber," in OSA Trends in Optics and Photonics (TOPS) 70, Optical Fiber Communication Conference Technical Digest, Postconference Edition (Optical Society of America, Washington, DC, 2002), 466-468.
4. G. Bouwmans, L. Bigot, Y. Quiquempois, F. Lopez, L. Provino, and M. Douay, "Fabrication and characterization of an all-solid 2D photonic bandgap fiber with a low-loss region (< 20 dB/km) around 1550 nm," Opt. Express **13**, 8452-8459 (2005).
5. B. Bahadur, *Liquid Crystals: Applications and Uses*, (World Scientific, 1990).
6. M. W. Haakestad, T. T. Larsen, M. D. Nielsen, H. E. Engan, and A. Bjarklev, "Electrically tunable photonic bandgap guidance in a liquid-crystal-filled photonic crystal fiber," IEEE Photon. Lett. **17**, 819- 821 (2005).
7. G. Ren, P. Shum, X. Yu, J. Hu, G. Wang, and Y. Gong, "Polarization dependent guiding in liquid crystal filled photonic crystal fibers," Opt. Commun. **281**, 1598-1606 (2008).
8. S. P. Guo and S. Albin, "Simple plane wave implementation for photonic crystal calculations," Opt. Express **11**, 167-175 (2003).
9. N. M. Litchinitser, S. C. Dunn, B. Usner, B. J. Eggleton, T. P. White, R. C. McPhedran, and C. M. d. Sterke, "Resonances in microstructured optical waveguides," Opt. Express **11**, 1243-1251 (2003).
10. J. Lagsgaard, "Gap formation and guided modes in photonic band gap fibres with high-index rods," J. Opt. A: Pure Appl. Opt. **6**, 798-804 (2004).
11. T. A. Birks, G. J. Pearce, and D. M. Bird, "Approximate band structure calculation for photonic bandgap fibres," Opt. Express **14**, 9483-9490 (2006).
12. J. Sun and C. C. Chan, "Effect of liquid crystal alignment on bandgap formation in photonic bandgap fibers," Opt. Lett. **32**, 1989-1991 (2007).
13. A. W. Snyder and J. D. Love, *Optical Waveguide Theory* (Chapman and Hall ,1983).
14. C. L. Xu, W. P. Huang, J. Chrostowski, and S. K. Chaudhuri, "A full-vectorial beam propagation method for anisotropic waveguides," J. Lightwave Technol. **12**, 1926-1931 (1994).
15. *Lixon Information*, (Chisso Corporation, Chiba, Japan, (1995).

1. Introduction

Photonic crystal fibers (PCFs) have attracted a lot of research attention since its first demonstration in 1996 [1]. Such fibers have opened up many possibilities and promising

#92705 - $15.00 USD Received 13 Feb 2008; revised 17 Mar 2008; accepted 18 Mar 2008; published 25 Apr 2008

applications in communication and sensing [2]. The presence of microstructured air holes around the fiber core has allowed more degrees of freedom in design than conventional fiber design. When the air holes are infiltrated with fluid material which has higher index than silica background, the index-guiding silica-air PCFs could turn into PBG PCFs [3,4]. Nematic liquid crystal (NLC) which is anisotropic material with rod-like molecules is a good infiltration candidate due to its thermal and electrical tunability [5]. It has been experimentally demonstrated that the external electrical field controls the orientation and alignment of the NLC molecules, which consequently tunes the spectral position of the bandgaps [6]. The LC filled PCFs (LCPCF) are finding potential applications in sensing and polarization monitoring owing to the thermal and optical properties of LC infiltrations.

In order to model such PBG fibers, numerical techniques such as planewave expansion (PWE) technique [7, 8] solves Maxwell's equations and computes the band structure of the fiber. The exact details of the bandgap formation in the fiber are provided in the band plot at the expense of computing time. On the other hand, simplified models which treat the fibers as anti-resonant reflecting waveguides are able to provide some important information of the fiber and are efficient in calculation [9, 10]. However the size of the low-index regions is not considered in such models, therefore the bandgaps obtained from the isolated high-index rod provide limited understanding of the fiber. A more comprehensive analytical method which takes care of the low-index regions has been proposed [11]. The method is desirable to treat photonic crystal fibers with a cladding of isotropic high index rods in a low index background. However, this method is insufficient for band structure analysis of PCFs with anisotropic high-index rods such as LCPCFs, where the anisotropy of the LC infiltrations shall be considered in order to understand the formation of the band structure. In [12], the bandgap formation of LCPCF is discussed, which provides a possibility of using the scalar equation for the bandgap calculation, but without giving sufficient information on the theoretical origins, derivations and final results of the analytical solutions. As it will be presented in this work, after the scalar eigenvalue equation has been modified and transformed, the analytical solutions can be expressed in Bessel functions.

In this paper, we extend the analytical approach of [11] to treat PCFs with high-index anisotropic materials immersed in low-index background materials. The anisotropy is considered in the analytical solutions of the field distribution by introducing a coefficient to describe the anisotropy of the NLC cells. This analytical method is therefore generalized to investigate the bandgap formation of photonic crystal fibers with high-index isotropic and anisotropic materials in low-index background. Based on the method, the influence of the degree of the NLC anisotropy as well as the index difference with the silica background on the bandgap properties is investigated.

2. Formulation of the analytical method

Figure 1(a) depicts the structure of the LCPCF investigated in the paper, Λ is the lattice constant and d is the diameter of the air hole, which is infiltrated with NLC molecules. Consider the cladding consists of infinite photonic crystal of the NLC rods embedded in silica background, the hexagonal unit cell is approximated to a circular cell as in Figs. 1(b), 1(c). The shaded circular rods represent air holes with NLC infiltrations. The radius of the approximated circular unit cell is obtained from the assumption that the high-index rods takes up the same fraction of the unit cell that $b = (\sqrt{3}/2\pi)^{1/2}\Lambda$ [11]. The refractive index of the NLC is a tensor n_{hi} and is described by extraordinary and ordinary refractive index of n_e and n_o respectively. For example, when NLC molecular are aligned along y- axis, $n_{hi} = \mathrm{diag}(n_o,n_e,n_o)$; when they are aligned along x- axis, $n_{hi}=\mathrm{diag}(n_e,n_o,n_o)$. The orientation of the NLC molecules can be controlled by appropriate homeotropic anchoring conditions or external electrical field [5, 6]. The approximated circular unit cell represents a typical cylindrical coordinate system which is defined by (r,δ) radial and azumithal axes. For small index contrast between n_{hi} and

#92705 - $15.00 USD Received 13 Feb 2008; revised 17 Mar 2008; accepted 18 Mar 2008; published 25 Apr 2008

n_{lo}, scalar weak-guidance approximation[13] is used to obtain the analytical solutions of the field distributions in the unit cell.

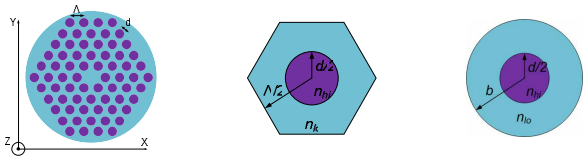

(a) (b) (c)

Fig.1. (a). LCPCF with triangular lattices. The shaded region in cladding is filled NLC, the background is silica. (b) Hexagonal unit cell of the NLC rods in silica. (c) Approximated circular unit cell of the NLC rods in silica

The eigenvalue equations of transverse electric fields are [14]

$$\begin{aligned}
&\frac{\partial^2\psi_x}{\partial y^2}+\frac{\partial}{\partial x}\left[\frac{1}{n_{zz}^2}\frac{\partial}{\partial x}\left(n_{xx}^2\psi_x\right)\right]+\left(n_{xx}^2k^2-\beta^2\right)\psi_x=\frac{\partial^2\psi_y}{\partial x\partial y}-\frac{\partial}{\partial x}\left[\frac{1}{n_{zz}^2}\frac{\partial}{\partial y}\left(n_{yy}^2\psi_y\right)\right]\\
&\frac{\partial^2\psi_y}{\partial x^2}+\frac{\partial}{\partial y}\left[\frac{1}{n_{zz}^2}\frac{\partial}{\partial y}\left(n_{yy}^2\psi_y\right)\right]+\left(n_{yy}^2k^2-\beta^2\right)\psi_y=\frac{\partial^2\psi_x}{\partial x\partial y}-\frac{\partial}{\partial y}\left[\frac{1}{n_{zz}^2}\frac{\partial}{\partial x}\left(n_{xx}^2\psi_x\right)\right]
\end{aligned} \tag{1}$$

where $\Psi_{x,y}$ represents the electric field distribution in the unit cell along x- and y- directions, k is the free space wavevector, β is the propagation constant. The coupling terms are neglected if low index contrast and low anisotropy are assumed [12]. In this work, we take n_{hi}=diag(n_o,n_e,n_o) for demonstration purpose, i.e. $n_{zz}=n_o$, $n_{xx}=n_o$ and $n_{yy}=n_e$. For x-polarized mode, it is fairly reasonable to assume $\Psi_y n_e^2 \approx \Psi_y n_o^2$ since $\Psi_y \ll \Psi_x$. Similarly for y- polarized mode we assume $\Psi_x n_o^2 \approx \Psi_x n_e^2$ since $\Psi_x \ll \Psi_y$[7]. A general expression in cylindrical coordinate system is derived for both polarizations as

$$\frac{\partial^2\psi}{\partial r^2}+\frac{f}{r}\frac{\partial\psi}{\partial r}+\left(k_0^2n_i^2-\beta^2-\frac{fl^2}{r^2}\right)\psi=0 \tag{2}$$

where r is the radial variation, l is integer which defines the azumithal variation of the modes to satisfy the eigenvalue equation, n_i is either n_e or n_o in the NLC region depending on the polarization, f is the coefficient which describes the degree of anisotropy of the NLC inclusions. Specifically in the NLC region, f =1 for x- polarized mode and n_e^2/n_o^2 for y-polarized mode; in the silica region, f =1 for both polarizations. Therefore for x- polarization Eq. (2) is exactly the same as in isotropic system where [11] can be used directly to calculate the band structure. On the other hand, the eigenvalue equation for y- polarized mode is the same as the uniaxial anisotropic system where n_{hi}=diag(n_e,n_e,n_o), which is not in the standard form with Bessel functions as solutions. Here we define $R=r\sqrt{k_0^2n_i^2-\beta^2}$ and look for a solution of the form $\Psi=ZR^{-\theta}$, Eq. (2) is expressed in the standard form with solutions of Bessel functions as

$$R^2\frac{\partial^2Z}{\partial R^2}+R\frac{\partial Z}{\partial R}+\left(R^2-m^2\right)Z=0 \tag{3}$$

where $\theta=(f-1)/2$, $m^2=fl^2+\theta^2$. It is noted that for x-polarization mode in the NLC region, as well as both polarizations in the silica cladding, the eigenvalue equations are identical with isotropic systems. Only for y-polarization mode in NLC rods the anisotropy coefficient is necessary to be introduced into the scalar eigenvalue equation. The general solutions of the scalar eigenvalue equation corresponding to LP_{lq} mode of the rod with radius a and assuming $\beta<kn_{hi}$ are

#92705 - $15.00 USD Received 13 Feb 2008; revised 17 Mar 2008; accepted 18 Mar 2008; published 25 Apr 2008

$$\psi(r)=\begin{cases} J_m(Ur/a)/(Ur/a)^{\theta} & r\le a \\ \left[AK_l(Wr/a)+BI_l(Wr/a)\right] & r>a,\beta-kn_{lo}>0 \\ \left[CJ_l(Qr/a)+DY_l(Qr/a)\right] & r>a,\beta-kn_{lo}<0 \\ \left[E(r/a)^l+F(r/a)^{-l}\right] & r>a,\beta-kn_{lo}=0,l\neq 0 \\ \left[G+H\ln(r/a)\right] & r>a,\beta-kn_{lo}=0,l=0 \end{cases} \quad \text{where} \quad \begin{aligned} V^2&=k_0^2a^2\left(n_{hi}^2-n_{lo}^2\right) \\ W^2&=a^2\left(\beta^2-k_0^2n_{lo}^2\right)=-Q^2 \\ U^2&=a^2\left(k_0^2n_{hi}^2-\beta^2\right)=V^2-W^2 \end{aligned} \tag{4}$$

$$\begin{aligned} A&=\left[WJ_m(U)I_{l+1}(W)+UI_l(W)J_{m+1}(U)-J_m(U)I_l(W)(m-\theta-l)\right]/U^{\theta} \\ B&=\left[WJ_m(U)K_{l+1}(W)-UK_l(W)J_{m+1}(U)+J_m(U)K_l(W)(m-\theta-l)\right]/U^{\theta} \\ C&=\left[UY_l(Q)J_{m+1}(U)-QJ_m(U)Y_{l+1}(Q)-Y_l(Q)J_m(U)(m-\theta-l)\right]\pi/2U^{\theta} \\ D&=\left[QJ_m(U)J_{l+1}(Q)-UJ_l(Q)J_{m+1}(U)+J_l(Q)J_m(U)(m-\theta-l)\right]\pi/2U^{\theta} \\ E&=\left(J_{m-1}(V)V+J_m(V)(l-m-\theta)\right)/2lV^{\theta} \\ F&=\left(J_{m+1}(V)V+J_m(V)(l-m+\theta)\right)/2lV^{\theta} \\ G&=J_{\theta}(V)/V^{\theta} \\ H&=-J_{\theta+1}(V)/V^{\theta-1} \end{aligned} \tag{5}$$

$\Psi(r)$ is with circular symmetry of any linear combination of $cos(l\delta)$ and $sin(l\delta)$. J_l, K_l, I_l and Y_l are Bessel functions, *A*-*H* are coefficients determined by the continuity of the ψ and ψ' at the boundaries of $r=a$. [11] states that the condition $\Psi'(b)=0$ and $\Psi(b)=0$ defines the top and the lower edge of the band respectively. Therefore the dispersion relation between β and k for given l, q could be obtained from finding the roots of the function $f(V,W^2)=0$. The solutions of the top of the band and the bottom of the band are defined as

$$f_{top}(V,W^2)=\begin{cases} AK_l'(W\alpha)+BI_l'(W\alpha) \\ CJ_l'(Q\alpha)+DY_l'(Q\alpha) \\ E\alpha^l-F\alpha^{-l} \\ H/\alpha \end{cases} \quad f_{bottom}(V,W^2)=\begin{cases} AK_l(W\alpha)+BI_l(W\alpha) & W^2>0 \\ CJ_l(Q\alpha)+DY_l(Q\alpha) & W^2<0 \\ E\alpha^l+F\alpha^{-l} & W^2=0,l\neq 0 \\ G+H\ln\alpha & W^2=0,l=0 \end{cases} \tag{6}$$

where K_l' represents the derivatives of K_l etc, $\alpha=a/b$. With the above presented formulation, this model is ready to calculate the band structure of the LCPCFs with both isotropic and anisotropic high-index rods in low-index background. It is noted that when dealing with isotropic material, the value of θ is zero, resulting the analytical solutions and the boundary conditions exactly the same as [11].

3. Bandgap analysis

The formulated method is used to calculate the band structure of an air-silica PCF with NLC infiltrations. The refractive index of silica background is assumed to be 1.45. The anisotropic NLC inclusions have ordinary and extraordinary refractive indices n_o = 1.4884 and n_e = 1.5803 respectively [15]. The NLC cells are assumed to be aligned homogeneously in the air holes along *y* axis so that n_{hi} = diag(n_o,n_e,n_o). The relative hole diameter $d/\Lambda = 0.4$. A full-vectorial planewave expansion method (PWE) is used to obtain the bandgap of the LC cladding as shown in Fig. 2(a). The shaded regions in dark green are the total bandgaps of the LC cladding, which is polarization independent [7]. The core line is drawn at n = 1.45 below which the fiber modes are supported in the LCPCF. The bandgap map of the LCPCF obtained from the analytical method is shown in Fig. 2(b), which resembles the important properties of the band plot in Fig. 2(a). The total bandgaps shaded in dark green which is the overlap region between the bandgaps of *x*- and *y*- polarization modes, shows a good agreement with PWE. It can be seen that the second photonic band in Fig. 2(b) represents LP_{11} mode, corresponding to TE_{01}, TM_{01} and HE_{21} modes in the full-vectorial solution. The degeneracy of

#92705 - $15.00 USD Received 13 Feb 2008; revised 17 Mar 2008; accepted 18 Mar 2008; published 25 Apr 2008

these three modes in the scalar approach makes them indistinguishable and merging into the same one. In addition, due to the anisotropy of the NLC, the bandgaps exhibits splitting behaviors for two polarizations which can be observed from both plots highlighted orange and cyan, that the bandgaps of *x*- and *y*- polarizations have independent operating zones which could be explored for single-mode single-polarization applications.

The width of the first bandgaps for both polarizations are calculated and compared as shown in Fig. 3. At short wavelengths, the gap widths of both polarizations obtained from our method agree very well with the PWE. In addition, the normalized propagation constants corresponding to the maximum gap width are identical from both methods. The relative error of the maximum gap width, which is defined as the ratio of difference to the value calculated by PWE, is 0.52% for *x*- polarization compared to 2.24% for *y*- polarization. This difference can be understood since low index contrast between n_{hi} and n_{lo} is assumed in the formulation. Here $n_{hi} = n_o$ for *x*-polarization and $n_{hi} = n_e$ for *y*-polarization, where n_o is smaller than n_e, which yields better accuracy for *x*-polarization in the calculation. At longer wavelengths, discernible deviations occur for both polarizations that the gap width is smaller than that obtained from PWE. The variation in band plot is interpreted as narrower gap in longer wavelength range, e.g. beyond the normalized wavelength 0.7 shown in Fig. 2. Moreover, the PWE plot has solutions at smaller $\beta\Lambda$, i.e. the bandgaps by PWE extend further into longer wavelengths, which is also shown in Fig. 2. The circular cell approximation in this analytical method is less appropriate for larger d/Λ, e.g. for $d/\Lambda = 0.8$, with all the other parameters unchanged, the relative error of the maximum gap width for the first y-polarization gap between two methods is 7.45%. The proposed method is suitable for low contrast structures, i.e. the increasing index contrast would incur less accuracy, e.g. for $d/\Lambda = 0.4$, n_o=1.6482, n_e=1.75, the relative error between two methods is found to be 6.45%.

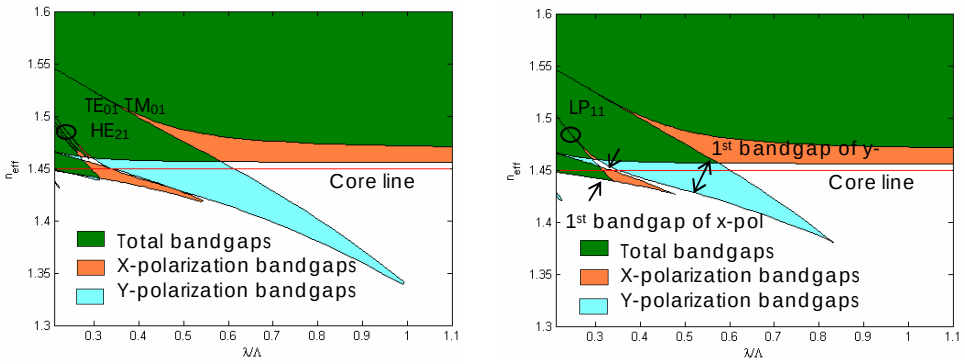

(a) (b)

Fig. 2. (a). Bandgap map of the LCPCF obtained from PWE method. (b). Bandgap map of the LCPCF obtained from the analytical method. The total bandgaps are the overlap zone between two polarization bandgaps.

#92705 - $15.00 USD Received 13 Feb 2008; revised 17 Mar 2008; accepted 18 Mar 2008; published 25 Apr 2008

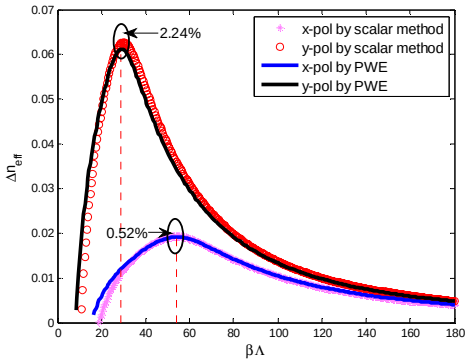

Fig. 3. Width of the first bandgap for both polarizations, obtained by the analytical scalar method and PWE method.

The presented method is used to investigate the bandgap properties under the influence of the different index contrasts. As an example, the first bandgap of *y*- polarization is studied. First of all, n_o is fixed at 1.4884, the ratio n_e^2/n_o^2 is increased from 1.0123 to 1.1274. As shown in Fig. 4(a), the increase in the ratio results in the red shift of the $\beta\Lambda$ corresponding to the maximum bandgap width indicated by the arrow. The red edge of the bandgap also shifts towards smaller value of $\beta\Lambda$ indicating that the bandgap penetrates further into longer wavelengths. The value of maximum gap width in terms of Δn_{eff} shows a monotonic rising trend with the increasing n_e^2/n_o^2 as shown in the inset. Figure 4(b) reveals the bandgap variations in terms of the normalized wavelength λ / Λ at two specific n_e^2/n_o^2 values, i.e. at 1.0123 and 1.1274 respectively. There is an evident red shift of the bandgap. The crossing points of the gap edges with the core line are used to describe the gap and are plotted as a function of n_e^2/n_o^2. The lower inset shows the rising trend of both red and blue edge of the gap with the ratio. The upper inset confirms the increase of the gap width with the ratio n_e^2/n_o^2. A qualitative explanation is that as the ratio keeps increasing, the polarization dependent bandgap splitting is more explicit which results in obvious red shifts of the gap. In summary, the increasing index difference between the n_e and n_o shifts the first bandgap to longer wavelengths, and broadens the bandgap width. Next, Figs. 4(c), 4(d) illustrate the variation of bandgap position and width under the influence of the ratio n_e^2/n_{si}^2. The n_e^2/n_o^2 is kept constant at 1.1274. Similar consequences of increasing ratios of n_e^2/n_{si}^2 on the bandgap are observed, but the variation of the position and the width of the bandgap are smaller.

#92705 - $15.00 USD Received 13 Feb 2008; revised 17 Mar 2008; accepted 18 Mar 2008; published 25 Apr 2008

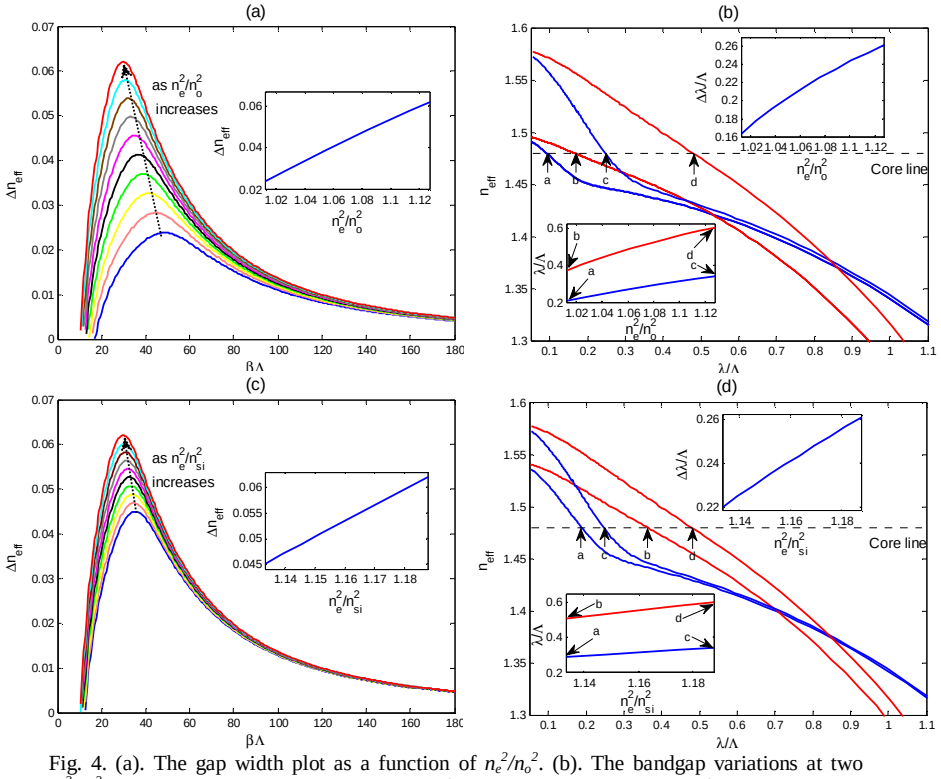

Fig. 4. (a). The gap width plot as a function of n_e^2/n_o^2. (b). The bandgap variations at two n_e^2/n_o^2 points. The insets show the variation of the position and the width of the gap. (c). The gap width plot as a function of n_e^2/n_{si}^2. (d). The bandgap variations in terms of the normalized wavelength. The insets show the variation of the position and the width of the gap.

4. Conclusions

We have presented a detailed demonstration of a simple analytical model for bandgap analysis for LCPCFs. Taking the anisotropy of the NLC into consideration, the coefficient of anisotropy is introduced into the explicit analytical solutions. The bandgaps calculated from the analytical method agree well with PWE results. It is found that the increasing anisotropy ratio of the NLC infiltrations and the increasing index difference with background silica both shift the first bandgap to longer wavelengths, and broadens the gap width. This method provides an efficient tool to the understanding of bandgap formation in LCPCFs, which are useful to aid the design based on such fibers.

Acknowledgments

This work is partially supported by Agency for Science, Technology and Research (A*STAR), Singapore.

#92705 - $15.00 USD Received 13 Feb 2008; revised 17 Mar 2008; accepted 18 Mar 2008; published 25 Apr 2008